Supporting Information for
"Anisotropic Interlayer Force Field for Heterogeneous Interfaces of Graphene and *h*-BN with Transition Metal Dichalcogenides"

Wenwu Jiang,[1#] Reut Sofer,[2#] Xiang Gao,[2#] Leeor Kronik,[3] Oded Hod,[2*]
Michael Urbakh[2], and Wengen Ouyang,[1,4*]

[1] *Department of Engineering Mechanics, School of Civil Engineering, Wuhan University, Wuhan, Hubei 430072, China*

[2] *School of Chemistry and The Sackler Center for Computational Molecular and Materials Science, Tel Aviv University, Tel Aviv 6997801, Israel*

[3] *Department of Molecular Chemistry and Materials Science, Weizmann Institute of Science, Rehovoth 76100, Israel*

[4] *State Key Laboratory of Water Resources Engineering and Management, Wuhan University, Wuhan, Hubei, 430072, China*

#: These authors contribute equally to this work.

[*] Corresponding authors. Email: w.g.ouyang@whu.edu.cn, odedhod@tauex.tau.ac.il

This supporting information document includes the following sections:

1. Low-Strain Sliding Potential Energy Surfaces

In the main text, the ILP is parameterized against binding energy (BE) curves calculated for low-strain configurations, as well as sliding potential energy surfaces (PESs) calculated for high-strain configurations. To examine whether this is sufficient for predicting the PES of low-strain configurations, we constructed a low strain (~2%) bilayer graphene/MoS_2 heterojunction and calculated the PES using both the PBE+MBD-NL and the ILP developed in this work. The results are shown in **Figure S1**. The PESs calculated using DFT exhibit corrugation lower than 0.01 meV/atom, which is below the expected accuracy of DFT and close to the numerical precision used. Strictly speaking, the ILP results show a lower corrugation (by about an order of magnitude) with a different PES pattern. However, we view this as numerically unimportant given the very small magnitude of the DFT corrugation.

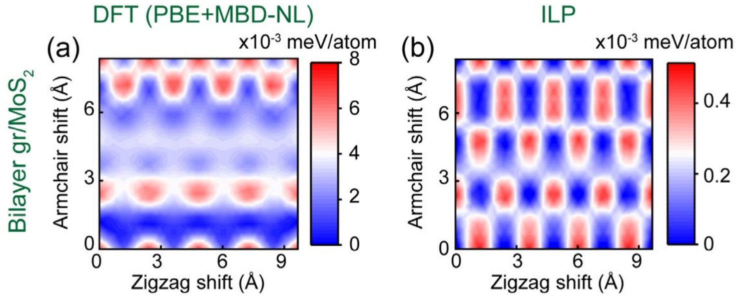

Figure S1. Sliding energy surfaces of a low strain (~2%) bilayer graphene/MoS_2 heterojunction, at a fixed interlayer distance of 4.2 Å, calculated using (a) PBE+MBD-NL, (b) ILP. The supercell, used also to obtain the results presented in the main text, contains 59 atoms (32 carbon, 9 molybdenum, and 18 sulfur atoms). The parameters of **Table S1** are used for the ILP calculations. The reported energies are normalized by the number of carbon atoms in the unit cell.

2. Interlayer Potential Form

In this section, we present the form of the parameterized ILP, which is the same as that used in our prior work on parameterized ILP for graphene, *h*-BN, and TMD systems.[1-3] The ILP contains a long-range vdW attraction term and a short-range registry-dependent Pauli repulsion term, denoted by $V_{\mathrm{att}}(r_{ij})$ and $V_{\mathrm{rep}}(\boldsymbol{r}_{ij},\boldsymbol{n}_i,\boldsymbol{n}_j)$, respectively, where i and j are indices of atoms in adjacent layers, at an interatomic distance $\boldsymbol{r}_{ij}$ (and $r_{ij}=|\boldsymbol{r}_{ij}|$), with local normal vectors of $\boldsymbol{n}_i,\boldsymbol{n}_j$ (see **Figure S2**). The ILP is then written in the following form:

$$V(\boldsymbol{r}_{ij},\boldsymbol{n}_i,\boldsymbol{n}_j)=\mathrm{Tap}(\boldsymbol{r}_{ij})\left[V_{\mathrm{att}}(r_{ij})+V_{\mathrm{rep}}(\boldsymbol{r}_{ij},\boldsymbol{n}_i,\boldsymbol{n}_j)\right], \tag{S1}$$

where

$$\mathrm{Tap}(r_{ij})=20\left(\frac{r_{ij}}{R_{\mathrm{cut}}}\right)^7-70\left(\frac{r_{ij}}{R_{\mathrm{cut}}}\right)^6+84\left(\frac{r_{ij}}{R_{\mathrm{cut}}}\right)^5-35\left(\frac{r_{ij}}{R_{\mathrm{cut}}}\right)^4+1, \tag{S2}$$

is a taper function that dampens the interactions between any pair of atoms i and j in different layers based on a cut-off distance R_{cut} (16 Å in our case). For the attractive potential, we use:

$$V_{\mathrm{att}}(r_{ij})=-\frac{1}{1+e^{-d_{ij}\left[r_{ij}/\left(s_{R,ij}\cdot r_{ij}^{\mathrm{eff}}\right)-1\right]}}\frac{C_{6,ij}}{r_{ij}^6}, \tag{S3}$$

where $C_{6,ij}$ is the pairwise vdW attraction coefficient, r_{ij}^{eff} is the sum of the effective equilibrium vdW atomic radii, and d_{ij} and $s_{R,ij}$ are unitless parameters determining the steepness and onset of a short-range Fermi−Dirac type damping function. For the anisotropic repulsive potential, we use:

$$V_{\mathrm{rep}}(\boldsymbol{r}_{ij},\boldsymbol{n}_i,\boldsymbol{n}_j)=e^{\alpha_{ij}\left(1-\frac{r_{ij}}{\beta_{ij}}\right)}\left\{\varepsilon_{ij}+C_{ij}\left[e^{-(\rho_{ij}/\gamma_{ij})^2}+e^{-(\rho_{ji}/\gamma_{ij})^2}\right]\right\}, \tag{S4}$$

where $\rho_{ij}(\rho_{ji})$ is the transverse (or lateral) distance, calculated as the distance of atom $j(i)$ to the surface normal, $\boldsymbol{n}_i(\boldsymbol{n}_j)$ of atom $i(j)$, namely:

$$\begin{cases}\rho_{ij}^2=r_{ij}^2-(\boldsymbol{r}_{ij}\cdot\boldsymbol{n}_i)^2\\ \rho_{ji}^2=r_{ji}^2-(\boldsymbol{r}_{ji}\cdot\boldsymbol{n}_j)^2\end{cases}. \tag{S5}$$

In the above ε_{ij} and C_{ij} are constants that define the energy scales corresponding to the isotropic and anisotropic repulsions, respectively, β_{ij} and γ_{ij} set the associated interaction ranges, and α_{ij} is a parameter that sets the steepness of the isotropic repulsion function.

For a given carbon (or B, N) atom j, its normal vector is calculated by averaging the three normalized cross products of the vectors connecting atom j to its three nearest neighbors. For a given TMD atom i, the surface normal vector $\boldsymbol{n}_i$ is calculated based on its six nearest neighbor atoms residing in the same sublayer,

$$\boldsymbol{n}_i = \frac{\boldsymbol{N}_i}{|\boldsymbol{N}_i|}, \boldsymbol{N}_i = \frac{1}{6}\left[\sum_{k=1}^{6}\left(\boldsymbol{r}_{k,i} \times \boldsymbol{r}_{k+1,i}\right)\right], \tag{S6}$$

where $\boldsymbol{r}_{k,i} = \boldsymbol{r}_k - \boldsymbol{r}_i, k = 1,2,\cdots 6$, and the summation is cyclic with $\boldsymbol{r}_{7,i} = \boldsymbol{r}_{1,i}$. **Figure S2** illustrates the definition of the surface normal of a surface chalcogenide atom and a transition metal atom. In total, the ILP form involves a set of nine symmetric pairwise parameters $\boldsymbol{\xi} = \{\alpha_{ij}, \beta_{ij}, \gamma_{ij}, \varepsilon_{ij}, C_{ij}, d_{ij}, s_{R,ij}, r_{ij}^{\mathrm{eff}}, C_{6,ij}\}$, i.e., $\alpha_{ij} = \alpha_{ji}$, etc.

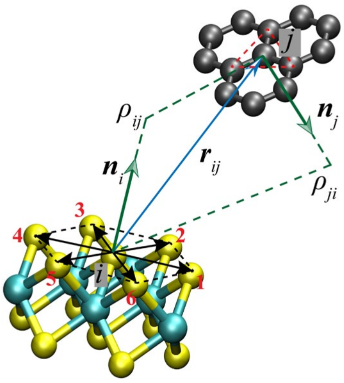

Figure S2. The definition of local normal vectors. For each atom i in the bottom layer (MX_2), its six nearest neighboring atoms within the same sublayer are chosen to define its normal vector $\boldsymbol{n}_i$. For each atom j in the top layer (graphene or *h*-BN), its three nearest neighboring atoms are chosen to define its normal vector $\boldsymbol{n}_j$.The distance vector and the lateral distances between atoms i and j residing in adjacent layers are marked by $\boldsymbol{r}_{ij}$ (blue arrow) and ρ_{ij} and ρ_{ji} (dashed green lines), respectively. The color scheme follows that used in **Figure 1** in the main text.

3. ILP Parameters

ILP parameters, fitted against the PBE+MBD-NL reference data as described in the main text, are presented in **Table S1**.

Table S1. List of ILP parameter values for laterally periodic bilayer graphene/MX_2 and bilayer *h*-BN/MX_2 (M = Mo, W; X = S, Se). The training set includes all PBE+MBD-NL bilayer BE curves and sliding PES data appearing in **Figures 2-4** of the main text. A value of $R_{\mathrm{cut}} = 16\ \text{Å}$ is used throughout.

	β_{ij} (Å)	**α_{ij}**	**γ_{ij} (Å)**	**ε_{ij} (meV)**	**C_{ij} (meV)**	**d_{ij}**	**$s_{R,ij}$**	**$r_{eff,ij}$ (Å)**	**$C_{6,ij}$ (eV·Å^6)**
C-Mo	2.5162	20.4549	25.1662	117.8104	94.2562	91.7401	0.4222	3.2733	103.7558
C-W	3.4722	20.8257	38.5879	119.1761	100.3990	91.7718	0.9603	3.5793	103.7302
C-S	3.1578	9.7355	1.8161	10.7498	33.4156	5.0013	1.8317	6.1774	409.3781
C-Se	3.3246	9.1122	1.3069	45.7186	16.6970	2.8007	2.4998	6.9996	409.3779
B-Mo	2.9153	32.0374	24.9785	128.1126	113.8054	86.4157	0.8368	4.2185	103.6475
B-W	3.4026	21.8385	24.5579	128.3749	114.6399	85.1473	1.0017	3.7279	103.6976
B-S	3.0171	11.3837	2.3665	0.3586	11.9733	5.0049	1.9760	4.6370	409.3807
B-Se	3.0943	15.2347	2.3288	0.0126	4.3560	2.5544	2.0812	5.4446	409.3807
N-Mo	2.9242	9.3663	21.6902	134.1419	126.3352	32.3692	1.2198	3.9220	103.6464
N-W	3.0398	8.6946	26.3310	71.3788	130.4323	68.1157	1.9885	2.4257	103.6944
N-S	2.8104	8.8804	2.2538	3.7179	141.3082	79.1573	2.2260	6.2481	409.3821
N-Se	2.9139	8.0162	1.0845	253.9939	38.2755	78.5764	2.2429	5.9342	409.3821

4. ILP for Benzene/MX_2 and Borazine/MX_2

Bilayer configurations of benzene/MX_2 and borazine/MX_2 are shown in **Figure S3**. Each bilayer system contains 120 atoms (108 atoms in the MX_2 and 12 atoms in the molecule). The size of the supercell was found to be large enough to avoid spurious interactions between the molecule and its periodic images. The interlayer distance is varied in the range of 4-12 Å for the BE curves. Each BE and sliding PES data set contains 35 and 132 data points, respectively.

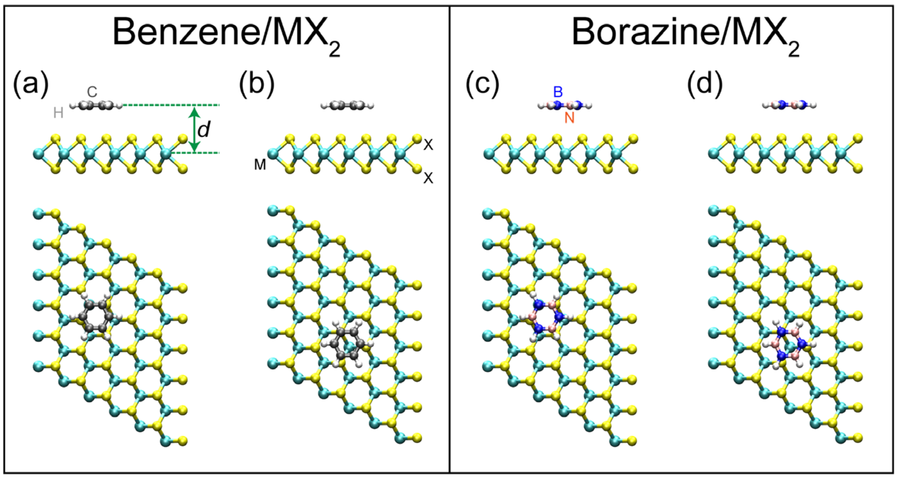

Figure S3. Stacking models of (a,b) benzene/MX_2 and (c,d) borazine/MX_2. In (a,c) the carbon or boron atom is located above the M atom, in (b, d) it is located above the X atom. All four systems are used to calculate reference BE data. For reference sliding PES data, only (a,c) are used. The gray, blue, pink, white, cyan, and yellow spheres represent carbon, boron, nitrogen, hydrogen, M (molybdenum or tungsten) and X (sulfur or selenium) atoms, respectively.

Figure S4 presents BE curves for the benzene/MX_2 and borazine/MX_2. All DFT calculations were again performed using PBE+MBD-NL, as implemented in the FHI-AIMS code,[4] with the tier-2 basis-set, choosing tight convergence settings with all grid divisions and a denser outer grid. Here, a vacuum of 100 Å is used with a *k*-point grid of 6×6×1 for all bilayer systems to prevent influence from image cells. Excellent agreement between the DFT and the fitted ILP is found.

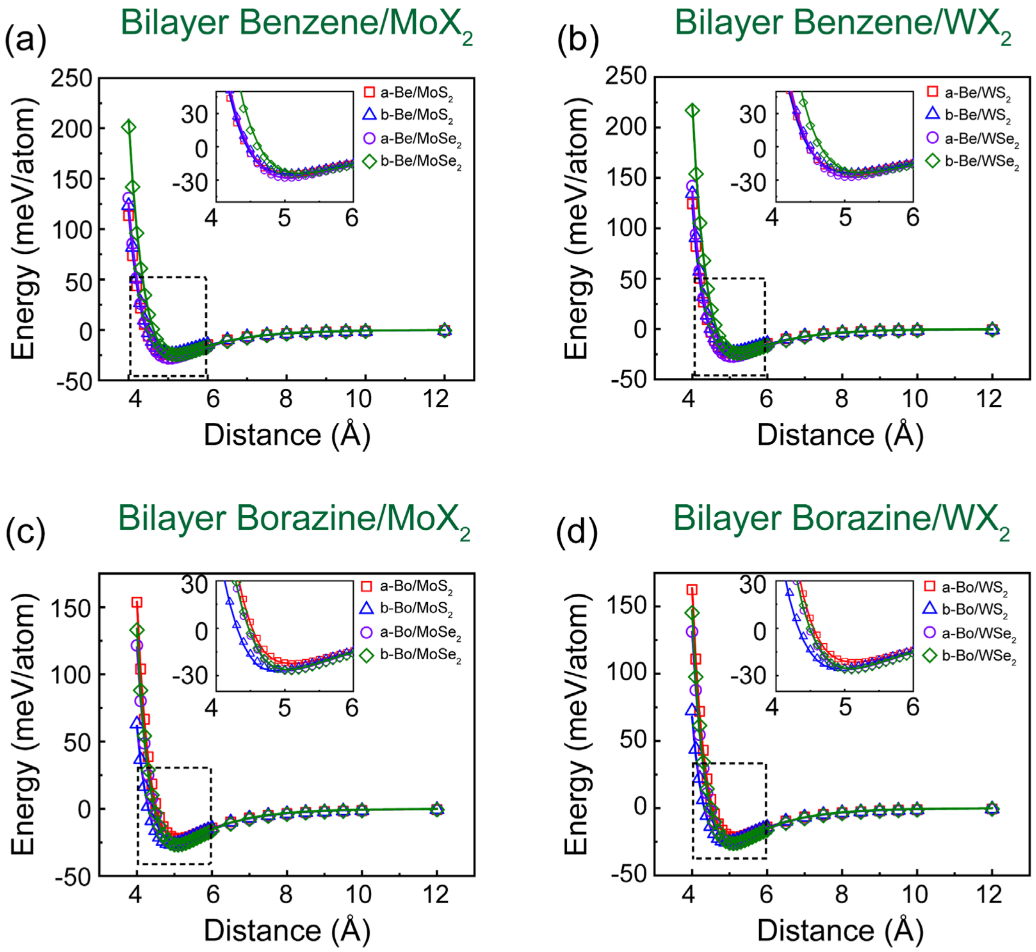

Figure S4. Binding energy curves for laterally periodic heterojunctions of (a,b) bilayer benzene/MX$_2$ and (c,d) bilayer borazine/MX$_2$ (M = Mo, W; X = S, Se), calculated using PBE+MBD-NL (open symbols), along with corresponding ILP fits (solid lines). Two different stacking modes (see **Figure S3**) are considered for each structure. The parameters presented in **Table S1** and **Table S2** of the SI are used to perform the ILP calculations. The reported energies are measured relative to the values of the initial two separated single layers and are normalized by the total number of molecule atoms in the unit-cell (12 atoms). The insets provide a zoom-in on the equilibrium interlayer distance region, marked by dashed black rectangles.

Sliding PES data for bilayer benzene/MX$_2$ and bilayer borazine/MX$_2$, calculated with PBE+MBD-NL at a fixed equilibrium interlayer distance (5.0 Å for benzene/MoS$_2$ and benzene/MoSe$_2$, 5.1 Å for the rest), are presented in the first row of **Figure S5** and **Figure S6**, respectively. The fitted ILP, given in the second row of these figures, agrees well with the PES DFT reference data, with differences (shown in the third row) within ~1.5 meV/atom.

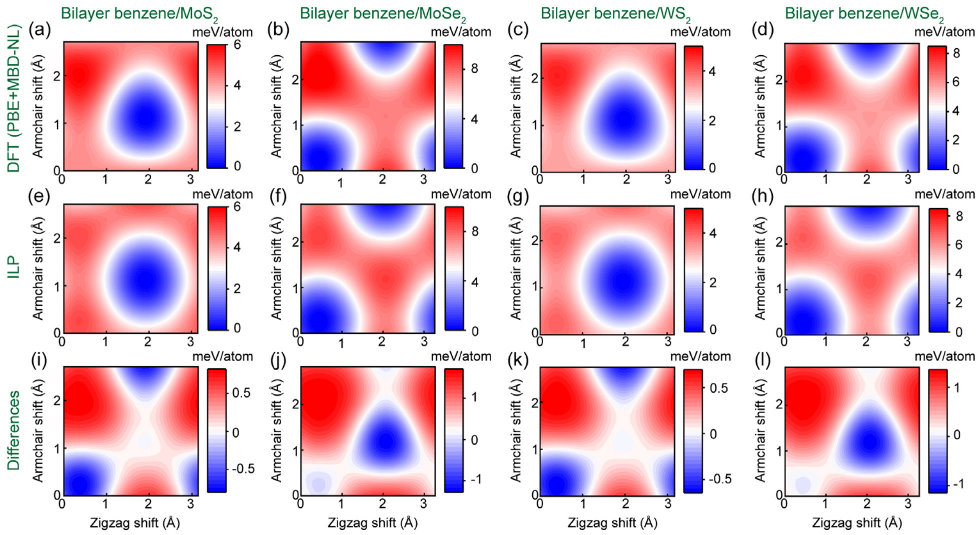

Figure S5. Sliding potential energy surfaces of laterally periodic bilayer benzene/MX$_2$ (M = Mo, W; X = S, Se) heterojunctions. First row: DFT reference data. Second row: fitted ILP data. Third row: Differences. Interlayer distances of 5.0 and 5.1 Å were used for the Mo and W containing bilayers, respectively. The parameters of **Table S1** above are used for the ILP, along with additional H-interaction parameters given in **Table S2**. The reported energies are normalized by the number of atoms in the benzene molecule (12 atoms).

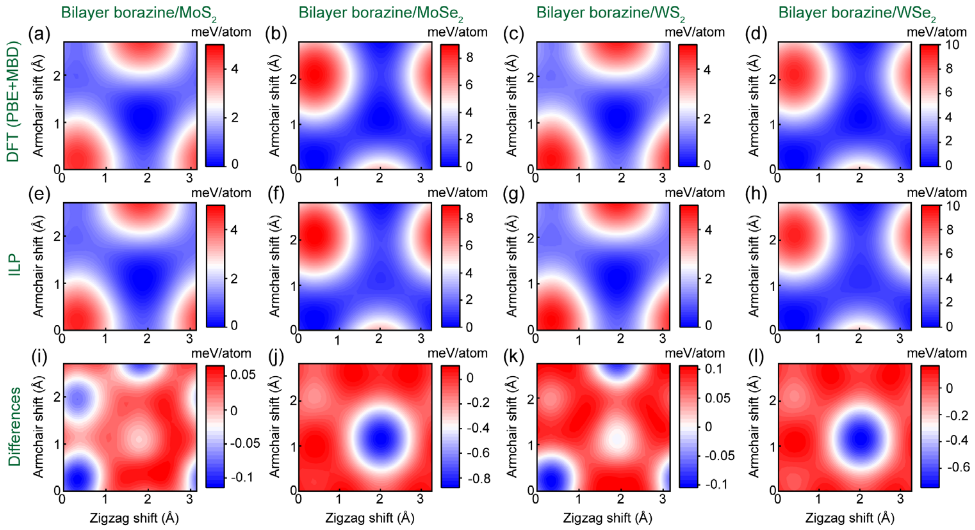

Figure S6. Sliding potential energy surfaces of laterally periodic bilayer borazine/MX$_2$ (M = Mo, W; X = S, Se) heterojunctions. First row: DFT reference data. Second row: fitted ILP data. Third row: Differences. An interlayer distance of 5.1 Å was used throughout. The parameters of **Table S1** above are used for the ILP, along with additional H-interaction parameters given in **Table S2**. The reported energies are normalized by the number of atoms in the benzene molecule (12 atoms).

Table S2. List of additional ILP parameters for laterally periodic bilayer benzene/MX_2 and borazine/MX_2 (M = Mo, W; X = S, Se). The training set includes all PBE+MBD-NL bilayer BE curves and sliding PES data of **Figures S4-S6.** A value of $R_{\mathrm{cut}} = 16$ Å is used throughout.

	β_{ij} (Å)	α_{ij}	γ_{ij} (Å)	ε_{ij} (meV)	C_{ij} (meV)	d_{ij}	$s_{R,ij}$	$r_{eff,ij}$ (Å)	$C_{6,ij}$ (eV•Å^6)
H-Mo	2.7823	7.6968	2.0190	243.3645	0.0290	98.9735	0.8946	5.2784	62.8329
H-W	2.9232	8.3797	8.9454	280.2233	36.2399	98.9716	1.7222	2.4879	62.0729
H-S	1.5797	2.1580	1.5691	0.0046	98.5879	10.7681	1.1314	4.3264	46.1562
H-Se	1.7964	2.0057	1.5320	58.0275	40.0042	15.7148	1.4697	2.4425	45.5459

5. Atomic Force Benchmark Test

To further ensure the reliability of the parameterized ILP, we performed additional DFT calculations to extract the total normal force acting on the graphene layer in the periodic graphene/MoS_2 bilayer at different interlayer spacings (blue circles in **Figure S7).** For comparison, we also calculated the same force-distance curve using the ILP (red curve in **Figure S7**) with the parameters presented in **Table S1**. Despite not being part of the reference dataset, the ILP force curve is in good agreement with the DFT results, with an average difference less than ~5.26 pN/atom across the entire interlayer distance range considered $(4 - 12\ \text{Å})$. This good agreement further demonstrates the transferability and robustness of the developed ILP.

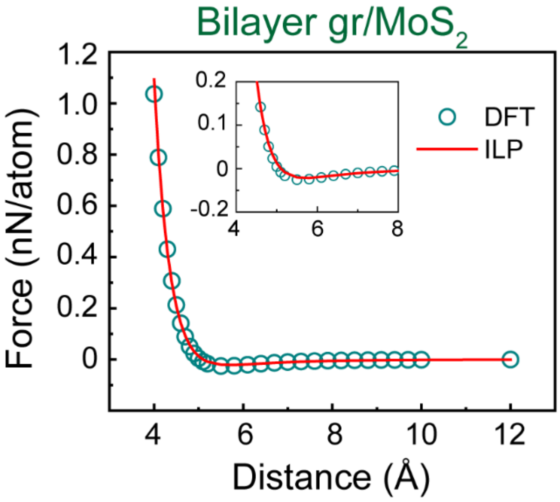

Figure S7. Total normal force as a function of interlayer distance calculate for the laterally periodic graphene/MoS_2 heterojunction using DFT (at the PBE+MBD-NL level of theory, blue open circles) and the ILP (solid red line). The forces are normalized by the total number of graphene atoms in the 2% strain supercell (32 in total). The insets provides a zoom-in on the equilibrium interlayer distance region.

6. Bulk Modulus Calculations

Figure S8 presents two bulk heterogeneous structures formed between MX_2 (M = Mo, W; X = S, Se) and graphene or *h*-BN, used for calculating bulk moduli. The first structure, referred to as (a) 16L-gr/MX_2 or (c) 16L-*h*-BN/MX_2, consists of 16 alternating layers of MX_2 and graphene or *h*-BN. The second structure, referred to as (b) 8L-gr/8L-MX_2 or (d) 8L-*h*-BN/8L-MX_2, is constructed by stacking an eight-layer graphene (AB stacking) or *h*-BN (AA′ stacking) slab atop an eight-layer MX_2 slab with AA′ stacking.

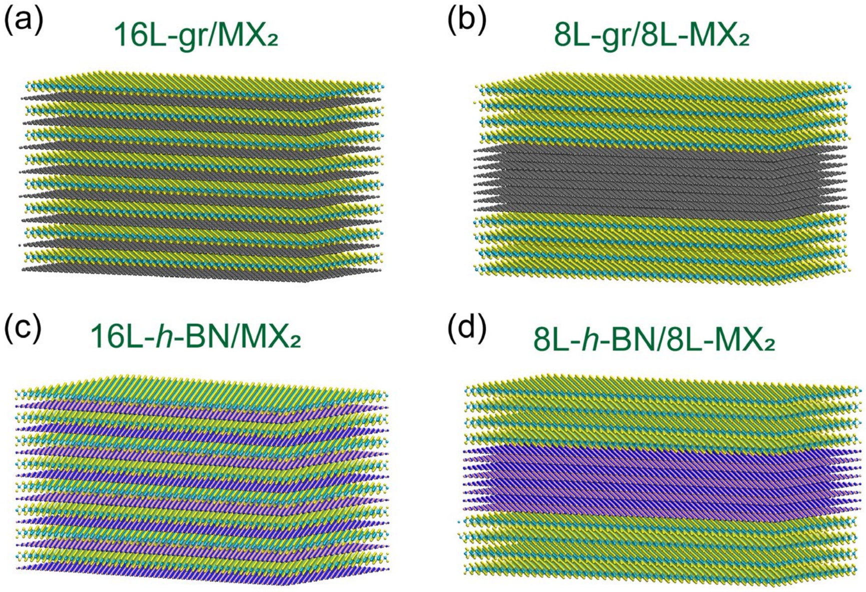

Figure S8. Snapshots of the (a) 16L-gr/MX_2, (b) 8L-gr/8L-MX_2, (c) 16L-*h*-BN/MX_2, and (d) 8L-*h*-BN/8L-MX_2 systems at zero pressure and 0 K. The gray, blue, pink, cyan and yellow spheres represent carbon, boron, nitrogen, M (molybdenum or tungsten) and X (sulfur or selenium) atoms, respectively.

Bulk moduli were extracted from the pressure-volume (P-V) curves (see **Figures 7-8** in the main text) using three equations of state (EOS): the Murnaghan equation (eq S7),[5, 6] the Birch-Murnaghan equation (eq S8),[7, 8] and the Vinet equation (eq S9),[9, 10] which take the following forms, respectively:

$$\frac{V}{V_0} = [1 + \frac{B_V'}{B_V^0} P]^{\frac{-1}{B_V'}}. \tag{S7}$$

$$P = 3B_V^0 \xi (1 + 2\xi)^{5/2} \left[1 - \frac{3}{2}(4 - B_V')\xi\right], \xi = \frac{1}{2}[\left(\frac{V}{V_0}\right)^{-\frac{2}{3}} - 1]. \tag{S8}$$

$$P = 3B_V^0 \frac{(1-X)}{X^2} \exp\left[\frac{3}{2}(B_V' - 1)(1 - X)\right], X = \left(\frac{V}{V_0}\right)^{\frac{1}{3}}. \tag{S9}$$

Here, V_0 and V are the unit-cell volumes in the absence and presence of external hydrostatic pressure, and B_V^0 and B_V' are the bulk modulus and its pressure derivative at zero pressure, respectively. The three equations differ in their description of the dependence of B_V' on the pressure, by assuming that it is linear, polynomial, and exponential for the Murnaghan, Birch-Murnaghan, and Vinet EOS, respectively.

7. Phonon Spectra of Bilayer Heterojunctions

Figure S9 shows phonon dispersion curves for bilayer graphene/MX_2 and *h*-BN/MX_2 (M = Mo, W; X = S, Se) heterojunctions, calculated using the ILP potential along with the Lennard-Jones potential. The intralayer potential is adopted as REBO,[11] Tersoff,[12] and Stillinger-Weber (SW)[13] potential for graphene, *h*-BN, and MX_2 (M = Mo, W; X = S, Se), respectively. The computed model contains 6×6×1 unit cells (2124 atoms). 201 *q* points were used to plot each branch of the phonon spectrum. We find that the choice of interlayer potential affects mostly the low energy phonon dispersion (around *Γ*-point) that corresponds to the interlayer phonon modes.

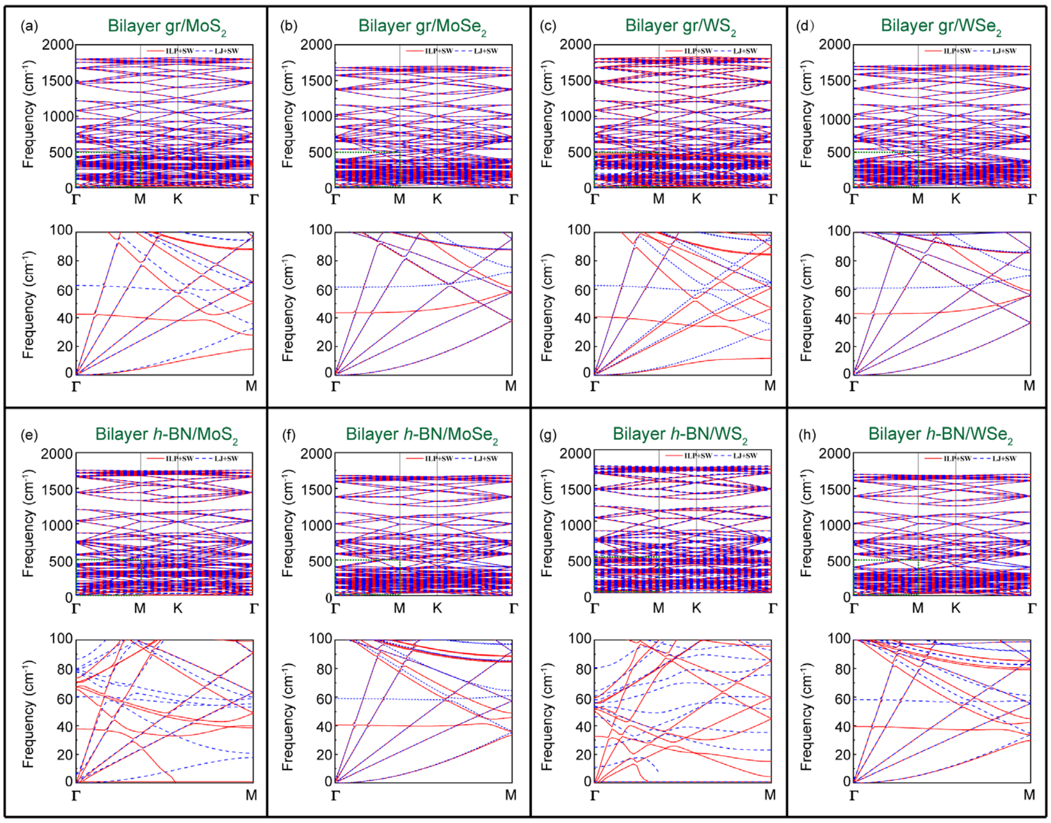

Figure S9. Phonon spectra of eight bilayer heterojunctions calculated using the ILP (red lines) and the LJ potential[14] (dashed blue lines).

8. Convergence Tests of the Reference DFT Calculations

To verify that binding energy (BE) results presented in the main text are convergence with respect to the basis set used, we constructed a high strain (~15%) graphene/MoS_2 bilayer and calculated the BE with the PBE+MBD-NL method, using the four tiers of numerical basis sets available within FHI-AIMS. The results shown in **Figure S10** demonstrate that the tier-2 basis-set used to obtain the results presented in the main text yields satisfactory convergence to within ~0.15 meV/atom.

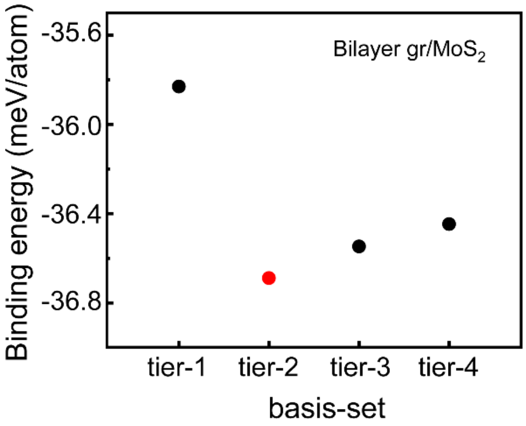

Figure S10. Binding energy (BE) for a strained (~15%) bilayer graphene/MoS_2 heterojunction, calculated at a fixed interlayer distance of 5.1 Å using the PBE+MBD-NL method as a function of the numerical basis set tier in FHI-AIMS. The supercell, which is the same as that used to obtain the results presented in the main text, contains 9 atoms (6 carbon, 1 molybdenum, and 2 sulfur atoms). The reported energies are normalized by the number of carbon atoms in the unit cell.

References

(1) Ouyang, W.; Azuri, I.; Mandelli, D.; Tkatchenko, A.; Kronik, L.; Urbakh, M.; Hod, O., Mechanical and Tribological Properties of Layered Materials under High Pressure: Assessing the Importance of Many-Body Dispersion Effects. *J Chem. Theory Comput.* **2020,** *16* (1), 666-676.

(2) Ouyang, W.; Sofer, R.; Gao, X.; Hermann, J.; Tkatchenko, A.; Kronik, L.; Urbakh, M.; Hod, O., Anisotropic Interlayer Force Field for Transition Metal Dichalcogenides: The Case of Molybdenum Disulfide. *J Chem. Theory Comput.* **2021,** *17* (11), 7237-7245.

(3) Jiang, W.; Sofer, R.; Gao, X.; Tkatchenko, A.; Kronik, L.; Ouyang, W.; Urbakh, M.; Hod, O., Anisotropic Interlayer Force Field for Group-VI Transition Metal Dichalcogenides. *J. Phys. Chem. A* **2023,** *127* (46), 9820-9830.

(4) Blum, V.; Gehrke, R.; Hanke, F.; Havu, P.; Havu, V.; Ren, X.; Reuter, K.; Scheffler, M., Ab initio molecular simulations with numeric atom-centered orbitals. *Comput. Phys. Commun.* **2009,** *180* (11), 2175-2196.

(5) Hanfland, M.; Beister, H.; Syassen, K., Graphite under pressure: Equation of state and first-order Raman modes. *Phys. Rev. B Condens. Matter.* **1989,** *39* (17), 12598-12603.

(6) Murnaghan, F. D., The Compressibility of Media under Extreme Pressures. *Proc. Natl. Acad. Sci. U.S.A.* **1944,** *30* (9), 244-247.

(7) Birch, F., Elasticity and constitution of the Earth's interior. *J. Geophys. Res.* **1952,** *57* (2), 227-286.

(8) Birch, F., Finite Elastic Strain of Cubic Crystals. *Phys. Rev.* **1947,** *71* (11), 809-824.

(9) Vinet, P.; Ferrante, J.; Smith, J. R.; Rose, J. H., A universal equation of state for solids. *J. Phys. C: Solid State Phys.* **1986,** *19*, L467-L473.

(10) Vinet, P.; Smith, J. R.; Ferrante, J.; Rose, J. H., Temperature effects on the universal equation of state of solids. *Phys. Rev. B Condens. Matter.* **1987,** *35* (4), 1945-1953.

(11) Donald, W. B.; Olga, A. S.; Judith, A. H.; Steven, J. S.; Boris, N.; Susan, B. S., A second-generation reactive empirical bond order (REBO) potential energy expression for hydrocarbons. *J. Phys.: Condens. Matter* **2002,** *14* (4), 783.

(12) Kınacı, A.; Haskins, J. B.; Sevik, C.; Çağın, T., Thermal conductivity of BN-C nanostructures. *Phys. Rev. B* **2012,** *86* (11), 115410.

(13) Jiang, J.-W., Misfit Strain-Induced Buckling for Transition-Metal Dichalcogenide Lateral Heterostructures: A Molecular Dynamics Study. *Acta Mech. Solida Sin.* **2019,** *32* (1), 17-28.

(14) Rappe, A. K., Casewit, C. J., Colwell, K. S., Goddard, W. A., and Skiff, W. M., UFF, a Full Periodic Table Force Field for Molecular Mechanics and Molecular Dynamics Simulations. *J. Am. Chem. Soc.* **1992,** *114*, 10024-10035.